Journal of Alloys and Compounds 499 (2010) 11–16

Contents lists available at ScienceDirect

Journal of Alloys and Compounds

journal homepage: www.elsevier.com/locate/jallcom

The influence of B variation on the electronic properties of $Al_3Ni_{20}B_x$ ($6 \leq x \leq 12$)

M. Elhadi[a], M. ElMassalami[a,*], H. Takeya[b], R.E. Rapp[a], F.A.B. Chaves[a], A. Elzubair[c]

[a] Instituto de Fisica, Universidade Federal do Rio de Janeiro, Caixa Postal 68528, 21945-972 Rio de Janeiro, Brazil
[b] National Institute for Materials Science, Tsukuba, Ibaraki 305-0047, Japan
[c] IME, Praca General Tiburcio 80, 22290-270 Rio de Janeiro, Brazil

ARTICLE INFO

Article history:
Received 12 February 2010
Received in revised form 1 March 2010
Accepted 3 March 2010
Available online 9 March 2010

PACS:
71.20.Lp
74.70.Dd
75.20.En
75.47.Np

Keywords:
Intermetallics
Nickel-based aluminides
Electronic structure
Thermodynamic properties
Thermal analysis

ABSTRACT

We investigated the influence of B variation on the structural, thermal, and electronic properties of the ternary intermetallics $Al_3Ni_{20}B_x$ ($x = 6, 7, \ldots, 12$). On increasing the metalloid content, the cubic unit-cell parameter (space group $Fm\bar{3}m$) is observed to increase linearly. Down to 2 K (for selected cases down to 120 mK), no evidence of superconductivity or (de)localized magnetism is observed in any of the studied samples; rather, all exhibit a nonmagnetic and metallic character. Furthermore, the Pauli susceptibilities, the coefficients of the specific heats, and the coefficients of the resistivities are found to correlate strongly (but non-montonically) with the percentage of the Ni content per unit formula (the Ni 3*d* band is the dominant contributor to the density of states $N(E_F)$). Such a non-monotonic evolution of the electronic properties is attributed to a corresponding non-monotonic character of the $N(E)$ curve within the neighborhood of E_F.

1. Introduction

It is remarkable that there are only less than half a dozen stable ternary compounds within the whole Al–Ni–B ternary phase diagram [1–5] and that these compounds are located within the Ni-rich side of the phase diagram; as such their electronic properties should reflect a strong influence of the 3*d* band of the Ni-subsystem since this band is the major contributor to the total density of states at the Fermi level, $N(E_F)$ [6–8].

In general, the NICKEL-based aluminides present technologically advantageous properties such as higher melting points, good thermal and electrical conductivities, higher mechanical strength and stiffness at elevated temperatures, and higher oxidation and corrosion resistance. Among the ternary Ni-based aluminides, the $Al_3Ni_{20}B_x (6 \leq x \leq 12)$ series (the so-called τ phase) is the most prominent one. It crystallizes in the $Cr_{23}C_6$-type structure with space group $Fm\bar{3}m$ [4,9,10] – see Table 1 – and this very structure is observed to be maintained even if the boron content is varied between 17 and 34 at.%: while B fully populates the 24*e* site in $Al_3Ni_{20}B_6$, it is suggested that the additional B in $6 > x \leq 12$ forms a double homonuclear bond [9,3]. Such a variation across this wide homogeneity range is expected to be accompanied by considerable variation in the electronic properties such as the bonding, magnetic, thermal, and transport properties: a modification in $N(E_F)$ causes change in these properties. Then, an experimental investigation on the correlation between the metalloid content and the physical properties of this series would be highly desirable. Fewer investigations were reported on the properties of this $Al_3Ni_{20}B_x$ series [11] and, to the best of our knowledge, none on the correlation of these properties with the B content.

This work reports on a systematic investigation of the influence of the B variation on the structural, thermal, magnetic, and electrical properties of the $Al_3Ni_{20}B_x (6 \leq x \leq 12)$ series. Intensive measurements were carried out on various samples and across wide ranges of temperature and magnetic field. Particular attention was paid to rationalize the experimental results in terms of the induced variation in $N(E_F)$.

2. Experimental

Stoichiometric amounts of $Al_3Ni_{20}B_x$, $Al_{2.5}Ni_{20.5}B_6$, and $Al_3Ni_{18}B_9$ phases – using pure Ni (99.9%), Al (99.9%), and B (99.8%) elements – were melted under argon atmosphere (99.9%) in conventional arc-melt or induction furnaces. Annealing of Ta-wrapped buttons of selected samples were carried out in a quartz tube and under argon atmosphere. Single-phase character of these τ phases were confirmed by structural analysis for both as-prepared and annealed samples. Since we

* Corresponding author. Tel: +55 21 25627320; fax: +55 21 25627368.
E-mail address: massalam@if.ufrj.br (M. ElMassalami).

0925-8388/$ – see front matter © 2010 Elsevier B.V. All rights reserved.
doi:10.1016/j.jallcom.2010.03.051

Table 1
Comparison of crystallographic structural parameters of some Ni-based τ- boride phases (space group *Fm*-3*m*). The lattice parameter are taken from the present work but the position, occupation and thermal parameters are taken from Ref. [4] and Inorganic Crystal Structure Data Base (2009). The quoted values of the position parameters are only indicative. The factor occ is the ratio of the multiplicity of the occupied positions to the general multiplicity. The additional B atoms, as quoted by Hillebrecht and Ade [4], are taken care of by a substitution of isolated boron atoms by B-pairs.

Composition	a (Å)	Al (4*a*)		Al (8c)		Ni (4*a*)		Ni (48*h*)		Ni (32*f*)		B1 (24*e*)	
		(*xyz*)	occ	(*xyz*)	occ	(*xyz*)	occ.	(*xyz*)	occ	(*xyz*)	occ	(*xyz*)	occ
$Al_3Ni_{20}B_6$	10.493(1)	(000)	$\frac{1}{48}$	$(\frac{1}{4}\frac{1}{4}\frac{1}{4})$	$\frac{1}{24}$	–	–	$(\eta\eta 0)$	$\frac{1}{4}$	$(\nu\nu\nu)$	$\frac{1}{6}$	$(0\zeta 0)$	$\frac{1}{8}$
$Al_{2.5}Ni_{20.5}B_6$	10.481(1)	(000)	$\frac{0.483}{48}$	$(\frac{1}{4}\frac{1}{4}\frac{1}{4})$	$\frac{1}{24}$	(000)	$\frac{0.517}{48}$	$(\eta\eta 0)$	$\frac{1}{4}$	$(\nu\nu\nu)$	$\frac{1}{6}$	$(0\zeta 0)$	$\frac{1}{8}$
$Al_3Ni_{20}B_{12}$	10.579(1)	(000)	$\frac{1}{48}$	$(\frac{1}{4}\frac{1}{4}\frac{1}{4})$	$\frac{1}{24}$	-	-	$(\eta\eta 0)$	$\frac{1}{4}$	$(\nu\nu\nu)$	$\frac{1}{6}$	$(0\zeta 0)$	$\frac{1}{8}$

$\eta \approx 0.169$, $\nu \approx 0.383$, $\zeta \approx 0.274$.

observed no drastic difference between the measured properties of the as-prepared and annealed samples, most of the obtained results (see below) were collected on as-prepared samples.

The thermal stability of all samples was evaluated (up to 1400 °C) by thermogravimetric analysis (TGA) and differential scanning calorimetry (DSC); both carried out under 99.9% argon atmosphere with a flow rate of 2 ml/min and a heating rate of 10 K/min. For all samples and within the experimental accuracy, TGA analysis up to 1400 ° C (not shown) revealed no noticeable weight loss.

Room-temperature powder diffractograms were collected on Cu Kα diffractometer. Crystal structure analysis was carried out using the Rietveld refinement method as implemented by the software package (`FullProf` suite) of J. Rodriguez-Carvajal. Due to our present experimental limitations (in monochromatization and slit correction), we were not able to refine the thermal and occupancy parameters. Rather the values reported in the literature were adopted. In spite of the above-mentioned limitations, the obtained *R*-factors are reasonable: $R_{wp} = 3$–7, while $\chi^2 = 2$–3.

The temperature-dependent specific heats on representative samples were measured on zero-field semi-adiabatic calorimeter which operates within the range $0.080 < T < 2$ K or $0.4 < T < 25$ K. Magnetization measurements were carried out on a magnetometer which operates within the ranges $1.9 \leq T \leq 300$ K and $H \leq 90$ kOe. Resistivities were measured within the ranges $1.9 < T < 300$ K on polycrystalline bars using the four-point method.

The analysis of the specific heat, magnetization and resistivity measurements were carried out using the theoretical expressions collected in Appendix A.

3. Results

3.1. Structural analysis

The diffractograms of $Al_3Ni_{20}B_x$ (Fig. 1) are in accord with the single-phase character of the τ-boride face-centered cubic structure, confirming the earlier conclusions [4,9] that the metalloid enters interstitially leading to a linear increase of the *a* parameter: $a = 10.393(5) + 0.017(1).x$ Å, reaching almost 1% increase as $x = 12$ (see Fig. 2): in agreement with the Vegards's law, the introduction of the incompressible metalloid leads to an isotropic volume expansion.

The structural (in general, electronic) properties of this series are expected to be influenced by two features which were reported to be common in this series [4]: the incorporation of a large number of point defects (such as vacancies or antisite atoms) and the considerable atomic interchange that can take place within the different crystallographic sites (see Table 1). We evaluated the influence of these two features on the structural properties of $Al_3Ni_{18}B_9$ and $Al_{2.5}Ni_{20.5}B_6$: Fig. 2 compares their lattice parameter with that of $Al_3Ni_{20}B_x$. It is evident that while a Ni vacancy in $Al_3Ni_{18}B_9$ does not modify the lattice parameter, a Ni substitution of Al in $Al_{2.5}Ni_{20.5}B_6$ leads to a considerable reduction in the lattice parameter. These conclusions highlight the importance of Al atoms in the determination of the unit-cell dimension.

3.2. Thermal analysis

Figure 3 shows the DSC curves of $Al_3Ni_{20}B_x$: unambiguous thermal events, occurring within the range 1000–1150 C, and manifested as strong and asymmetric peaks for $x \to 6$ but weak and resolved ones for $x \to 12$. Many processes (such as melting, structural phase transformation, atomic hopping,. . .) may contribute to these thermal events. In the lack of complementary studies (such as diffraction experiments), it is hard to elucidate the nature of these events. Nonetheless, based on Fig. 3, we were able to identify and follow the influence of the B incorporation on the intensities and temperatures of these events and, furthermore, to check whether there is any correlation between these events and the progressive addition of B.

The asymmetric character of these transformations suggests a multi-peaks feature most probably driven by distinct thermal processes. We, empirically, approximated these events by three superposed Gaussians (Figs. 3 and 4) each with a peak center at $k_B T_{th}/e \approx 99.8$, 100.7, and 101.4 meV: these are denoted, respectively, as a low-T_{th}, mid-T_{th}, and high-T_{th} process.

Some general features can be inferred from the thermal evolution of these processes. While each of T_{th} decreases with B content [Fig. 4(a)], the evolution of the associated enthalpies differs greatly: Fig. 4(b) shows that as $x \to 12$, the intensity of the low-T_{th} (high-T_{th}) process increase (decreases) from (to) zero. In contrast, the enthalpy of mid-T_{th} process (as well as the total enthalpy) remains almost constant. These features suggest the followings: while the mid-T_{th} event can be attributed to a process that has no dependence on the additional B content, both the high-T_{th} and low-T_{th} events must be related to the act of adding more B in such an extent that

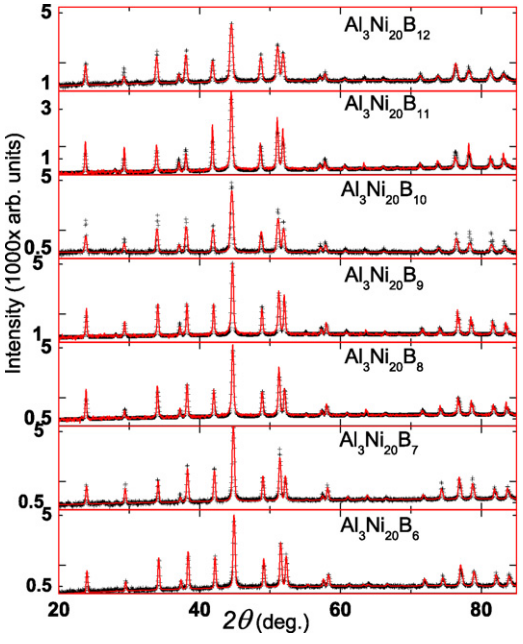

Fig. 1. Diffractograms of $Al_3Ni_{20}B_x$ ($x = 6, 7, \ldots, 12$). Logarithmic scale is used for the intensity axis. The experimental points (symbols) compares favorably with the theoretical intensity (solid lines) based on Rietveld calculation.

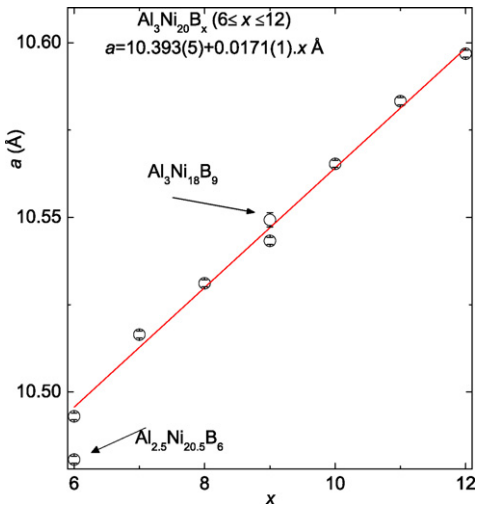

Fig. 2. The a-parameter of the τ-borides $Al_3Ni_{20}B_x$ as obtained from structural analysis of experimental diffractograms such as the ones shown in Fig. 1. The solid line is a least-square linear fit. Space group, atomic positions are given in Table 1. The data of $Al_3Ni_{20}B_6$ are in good agreement with Ref. [4]. For comparison, the lattice parameter of $Al_3Ni_{18}B_9$ and $Al_{2.5}Ni_{20.5}B_6$ are also included (see text).

while the low-T_{th} process is being activated and enhanced that of the high-T_{th} is being suppressed and, finally, blocked.

Basic thermodynamics considerations suggest that each of these thermal events can be characterized as an isobaric ($dp = 0$) process with no change in the number of involved particles (based on TGA results, $dN = 0$). Then the difference in the enthalpy can be expressed as:

$$\Delta H_{p,n} = T_{th}.\Delta S = k_B T_{th}.\ln\left(\frac{W_a}{W_b}\right) = E_A \ln\left(\frac{W_a}{W_b}\right) \quad (1)$$

where ΔS is the change in the entropy (see Table 2), $E_A = k_B T_{th}$ is the activation energy, and W_a (W_b) is the number of configuration available for the system above (below) T_{th}. Accordingly, the large value of ΔH_p is an indication that the ratios W_a/W_b and thus the amount of disorder is greatly enhanced after the thermally assisted process.

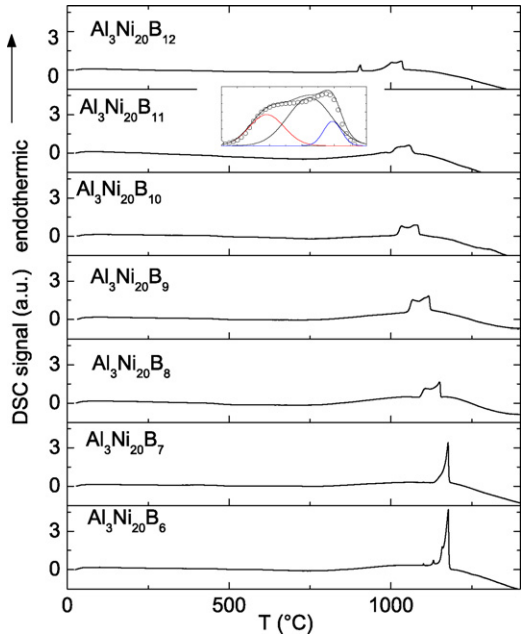

Fig. 3. DSC curves of $Al_3Ni_{20}B_x$ samples. For low B-content, the peaks are closer together and, as such, give rise to strongly asymmetric shapes. A very weak peak at the lower-side of the main event is evident only in the $x = 6$ and 12 samples and, as such, will not be considered further. Inset: an empirical decomposition of the main asymmetric event into three Gaussian peaks (see text).

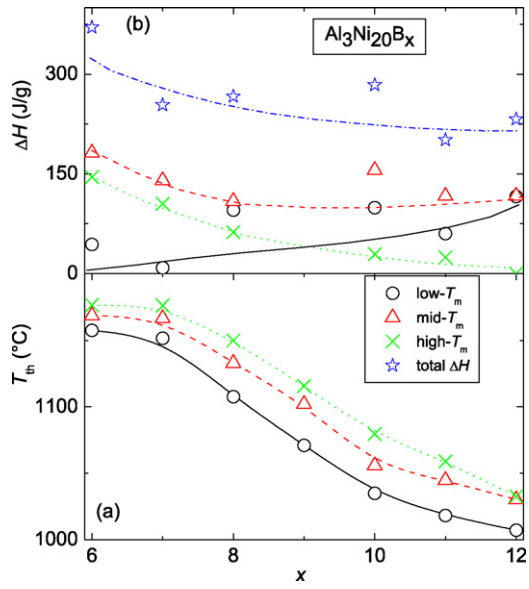

Fig. 4. The correlation of the B content in $Al_3Ni_{20}B_x$ with (a) the transition points T_{th} (center of the Gaussian peak) and (b) the amount of enthalpy, ΔH, (the area under the Gaussian peak) associated with the endothermic transformations shown in Fig. 3. The lines are a guide to the eyes.

3.3. Magnetization

It was observed that all the measured susceptibilities can be described as:

$$\chi_{dc} = \frac{M}{H} = \frac{C}{(T - \theta_{CW})} + \chi_o, \quad (2)$$

where the Curie–Weiss tail evaluates to an extremely weak value: $C \approx 10^{-4}$ emu/mole which amounts to a tiny effective contaminating moment of 0.03 μ_B per unit formula and $\theta_{CW} \approx 1$ K. χ_o is the temperature-independent susceptibility and the thermal evolution of which is shown in Fig. 5: the obtained χ_o (see Fig. 6 and Section 4) are all positive, small, and temperature independent indicating an absence of magnetic polarization of the Ni 3d band. This inference is in agreement with the finding of Hirota [11] that $Al_3Ni_{20}B_6$ is nonmagnetic. Moreover, it is consistent with the fact that most of the parent binary Al–Ni compounds are nonmagnetic [12]: the weak itinerant ferromagnetism of $AlNi_3$ disappears on an addition of only a very small percentage of B. Hase [6] showed that if $AlNi_3B$ exists, then it must be nonmagnetic since (in contrast to the ferromagnetic $AlNi_3$) its 3d band is shifted downwards away from E_F and, as a consequence, exhibits a lower $N(E_F)$ (see Fig. 2 of Ref. [6]).

Table 2
Comparison of the thermodynamical properties that are involved in the thermal event of the limit compound $Al_3Ni_{20}B_6$.

Compound	$Al_3Ni_{20}B_6$		
Event	Low-T_{th}	Mid-T_{th}	High-T_{th}
T_{th} (K)	1158	1169	1176
k_BT_{th}/e (meV)	99.8	100.7	101.3
ΔH (J/g)	43.8	181.6	145.2
ΔS (mJ/gK)	37.8	155.3	123.5

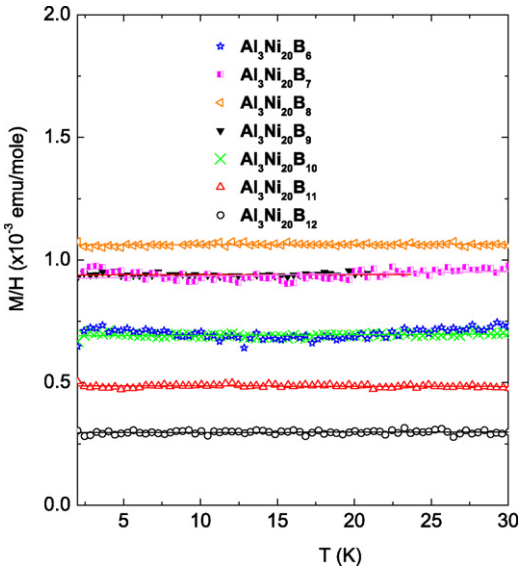

Fig. 5. DC susceptibilities ($\chi_o = M/H$) of $Al_3Ni_{20}B_x$. Two thermal scans were carried out, one during the warming cycle after zero-field cooling and another, directly afterwards, during cooling down to 2 K using the same 200 Oe. These curves were obtained after subtracting the weak contaminating signal using Eq. (2) (see text). The evolution of χ_o with Ni content is shown in Fig. 6.

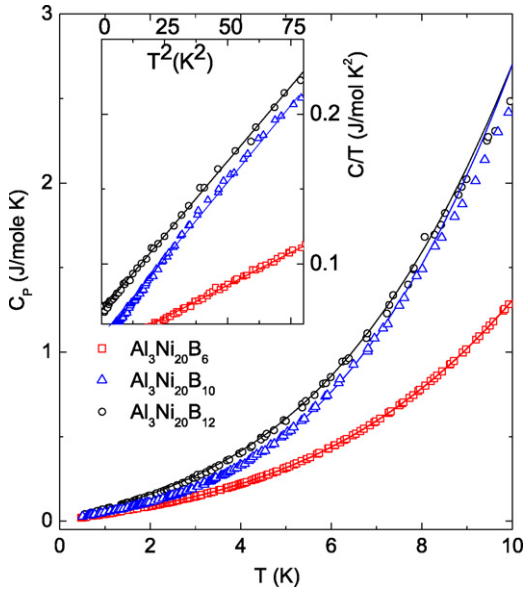

Fig. 7. The specific heat curves of representative $Al_3Ni_{20}B_x$ samples. Symbols represent measured values while solid lines are fits to Eq. (A.1) (the fit parameters are given in Fig. 6). The inset shows C/T *versus* T^2 of the curves shown in the main panel.

3.4. Specific heat

Each of the measured specific heat curves (see Fig. 7) follows faithfully Eq. (A.1) from which γ and β (and consequently θ_D) were determined. It is noted that both γ and θ_D do exhibit a correlation with the B content but their evolution is opposite to one another (see Fig. 6 and Section 4 below). Roughly speaking, γ varies around 50 mJ/mol K^{-2} which is smaller than what would be expected if the Ni-subsystem in these τ-phases contributes to $N(E_F)$ the same amount as the one reported for the elemental Ni [13]. Accordingly, it is suggested that the center of the 3*d* band is positioned well below E_F. θ_D, on the other hand, varies between 260 and 400 K indicating that the B addition has an appreciable influence on the elastic properties. Finally, as θ_D is expected to be proportional to the square root of the melting point [13], then the observation that T_{th} of Fig. 4 does not follow the same trend as that of θ_D [Fig. 6(c)] can be interpreted to mean that the T_{th} events should not be identified as melting processes.

3.5. Resistivity

The resistivities are metallic (Fig. 8) and, down to 2 K, exhibit no trace of superconductivity or any feature that can be attributed to a martensitic transformation [14] usually observed in quenched

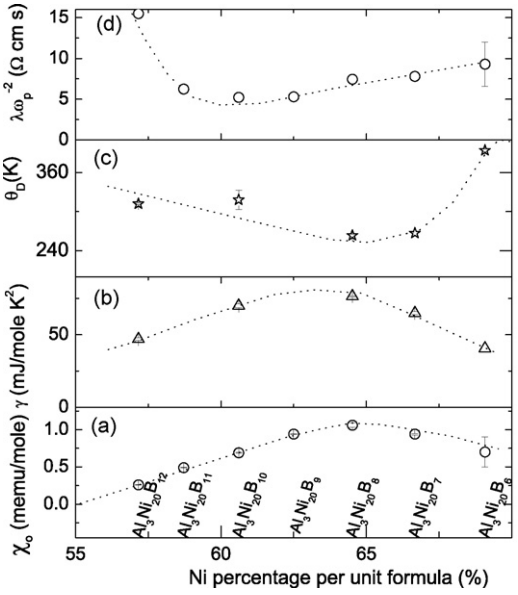

Fig. 6. The evolution of (a) the temperature-independent magnetic susceptibility χ_o, (b) the Sommerfeld coefficient γ, (c) the Debye temperature θ_D, and (d) the factor $\lambda\omega_p^{-2}$ (see Eq. (A.7)) as a function of the atomic percentage of Ni in each formula unit of $Al_3Ni_{20}B_x$. The error bars give the range of values obtained from different samples that were prepared by different synthesis routes. The (dotted) lines are a guide to the eyes.

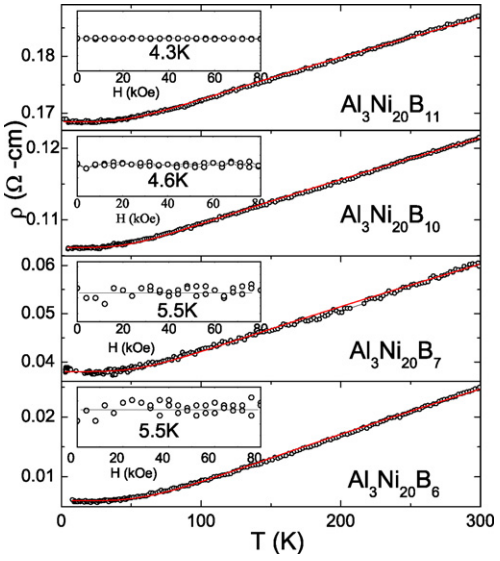

Fig. 8. Thermal evolution of the resistivities of representative $Al_3Ni_{20}B_x$ samples. The solid lines represent the calculation based on Eq. (A.7): as θ_D is taken from the specific heat analysis and ρ_0 is the residual resistivity, then the only free parameter is $\lambda\omega_p^{-2}$, the value of which is given in Fig. 6. The insets shows the magnetoresistivities of these samples: the y scale of each insert spans an interval of ±5% of each of the magnetoresistivity curve.

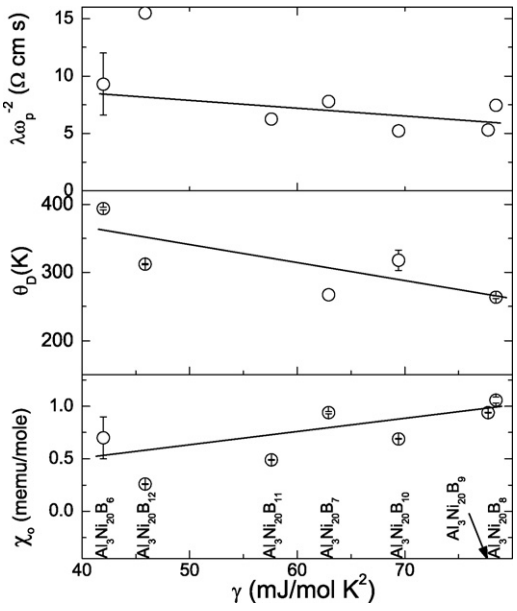

Fig. 9. Correlation of the measured γ with the measured values of χ_o (lower panel), θ_D (mid panel) and $\lambda\omega_p^{-2}$ (top panel) of $Al_3Ni_{20}B_x$ series (see Fig. 6 and the text).

Ni-rich aluminide phases. The measured curves compare favorably with the calculation of the Bloch–Gruneissen model (see Eq. (A.7)): in fact the thermal variation across $2 \leq T \leq 300$ K of all studied samples can be reproduced by varying only the ratio (λ/ω_p^2), ρ_0, and θ_D (with θ_D being fixed to the value obtained from the specific heat measurement). Based on this analysis, the overall coupling factor $(\lambda/\omega_p^2)\omega_D \simeq 3.10^{-7}$ Ω-cm.

The magnetoresistivity curves measured at liquid helium temperature and for field up to 90 kOe are shown in the insets of Fig. 8: within the experimental accuracy, the field-dependence of the electronic degrees of freedom is extremely weak emphasizing once more the absence of polarization of the Ni-subsytem.

4. Discussion: evolution of γ, χ_o, θ_D, $\lambda\omega_p^{-2}$

Taylor [12] showed that the magnetic properties of the binary aluminides can be understood in terms of their $N(E_F)$: a direct consequence of the fact that the Pauli contribution is dominant and that $N(E_F)$ appears in the expressions of χ_o (Eq. (A.6)). This statement can be generalized to the case of $Al_3Ni_{20}B_x$: their magnetic, thermal, and transport properties should manifest an orderly correlation with $N(E_F)$. In particular as γ is a linear function of $N(E_F)$, then all these measured properties should scale with γ: indeed Fig. 9 demonstrates that χ_o, θ_D, and $\lambda\omega_p^{-2}$ correlate almost linearly with γ. Evidently the evolution of χ_o is in accord with Eq. (A.6) while the decrease in the trend of $\lambda\omega_p^{-2}$ (when confronted with Eq. (A.7)) suggests that the increase in ω_p^2 is much stronger than that of λ.

Electronic structure calculations (e.g. Refs. [7,15,8]) on binary aluminides demonstrated that there is a charge transfer from Al to the 3*d* band of Ni and that the partial contribution of the Ni 3*d* orbitals, $N_{3d}(E_F)$, relative to the total $N(E_F)$ increases with the atomic percentage of Ni within the unit formula. Furthermore, Kulikov et al. [8] reported that the total $N(E_F)$ of $Al_{0.5-\delta}Ni_{0.5+\delta}$ ($\delta = -0.1, 0, 0.1$) increases with δ. Along similar line of arguments, we expect the main contribution to $N(E_F)$ of $Al_3Ni_{20}B_x$ to be from $N_{3d}(E_F)$ which in turn is correlated with the Ni percentage. As that the band structures of $Al_3Ni_{20}B_x$ are expected to remain unaltered when x is varied, then the variation in their electronic properties can be discussed in terms of a rigid-energy-band scenario. Consequently, if the decrease in the B content (from $Al_3Ni_{20}B_{12}$ toward $Al_3Ni_{20}B_6$) is a measure of an increase in the electron count, then the evolution of the electronic properties across $Al_3Ni_{20}B_x$ must reflect the shape of the $N(E)$ curve in the neighborhood of E_F. Accordingly, the non-monotonic evolution of χ_o, γ and $\lambda\omega_p^{-2}$ with the Ni percentage (see Fig. 6) is taken to be a reflection of the actual shape of the $N(E)$ curve.

It is emphasized that any variation in the electron–phonon interaction or electronic correlations would also influence the evolution of the measured electronic properties. Additionally, variation in the elastic parameters would influence mainly the evolution of θ_D and $\lambda\omega_p^{-2}$: this may explain the observation that the evolution of θ_D and $\lambda\omega_p^{-2}$ is opposite to that of χ_o and γ (see Fig. 6).

Transition metals are well known for their higher θ_D and melting points and these features are usually associated with the 3*d* band contribution. For $Al_3Ni_{20}B_x$, the weak lowering of θ_D with $N(E_F)$ (see Fig. 9) suggests the presence of other factors (in addition to the 3*d* contribution) such as (i) some antibonding states are being gradually filled as $N(E_F)$ is increased, (ii) *d* bonding is gradually weakened as Ni atoms are being separated by alloying, (iii) hybridization of the *p* band of B/Al with the Ni *d* band leads to a covalent contribution such as the one suggested for the binary Al–Ni intermetallics [7,15]. Then due to such possible competing influences, bonding properties may manifest non-monotonic dependence on B content: while the *p*-*d* hybridization increases with B content (thus stronger on the $Al_3Ni_{20}B_{12}$ side), the 3*d* band contribution increases with $N(E_F)$ (consequently, stronger on the $Al_3Ni_{20}B_6$ side).

Finally, considering the values of $N(E_F)$ as well as a possible introduction of higher phonon frequencies due to the addition of B, we searched for any possible surge of superconductivity in these phases. Measurements down to 2 K (in some cases down to 120 mK) on the titled compounds showed no trace of superconductivity. Within the BCS scenario, this absence is indicative of a weaker electron–phonon coupling, a weaker $N(E_F)$, or a smaller θ_D. Additionally, the above-mentioned large contribution of N_{3d} (E_F) to $N(E_F)$ may be accompanied by pair-breaking spin-fluctuation effects. Such spin fluctuations may be the reason behind some enhancement of the magnetic susceptibility (see Figs. 5 and 6).

In summary, we synthesized and investigated the structural, thermal, magnetic, and transport properties of $Al_3Ni_{20}B_x$ series. The cubic structure is maintained across the whole homogeneity range and, furthermore, the cubic lattice parameter evolves linearly with B content indicating that such an isotropic expansion is dominated by the size effect of the incompressible metalloid. A systematic correlation between the measured electronic properties and $N(E_F)$ has been uncovered: the evolution of the measured electronic properties across the homogeneity range does not show a monotonic evolution with either the B or Ni content. Such a non-monotonic character is taken to be indicative of a non-monotonic evolution of $N(E)$ curve within the neighborhood of E_F.

Acknowledgments

We acknowledge the partial financial support from the Brazilian agencies CNPq and Faperj and also ElNileen University (Sudan) for the financial support of M. Elhadi.

Appendix A. Some theoretical expressions used in data analysis

The measured low-temperature molar specific heat, C, is analyzed as a sum of an electronic and a lattice contribution:

$$C(T) = \gamma T + \beta T^3, \tag{A.1}$$

where the Debye coefficient β is:

$$\beta = \frac{12\pi^4 z N_A k_B}{(5\theta_D^3)}, \tag{A.2}$$

k_B is the Boltzmann constant, N_A Avogadro number, z is the number of atom per unit formula, and θ_D is the Debye temperature. The Sommerfeld factor γ is given as [13]:

$$\gamma = \frac{2}{3}\pi^2 k_B^2 N(E_F) = \frac{4\pi^3 m k_B^2}{3h^2}\left(\frac{3n_e N_A V_c^2}{Z^2}\right)^{1/3} \tag{A.3}$$

$$\simeq 9.7 \times 10^{-5}\left(\frac{\sqrt{n_e}.V_c}{Z}\right)^{2/3} \mathrm{J/mol\,K^2} \tag{A.4}$$

In the second line, $N(E_F)$ is replaced by its ideal electron gas expression and as such γ is a function of the unit cell volume V_c (in units of $\mathrm{\AA}^3$), the number of unit formula per unit cell Z, and the effective number of free electrons per unit formula n_e. As well known, such a free-electron expression is not appropriate for the description of the electronic properties of the 3*d* transition-metal based intermetallics: for the particular case of elemental Ni, Eq. (A.4) can be rearranged to express the product $(m^*/m)n_e^{(1/3)}$ (m^* is the effective mass) in terms of its measured $\gamma_{Exp} = 7.3\,\mathrm{mJ/K^{-2}}$ mole as:

$$\left(\frac{m^*}{m}\right).n_e^{1/3} = \frac{\gamma_{\mathrm{Exp}}}{9.7 \times 10^{-5}(.V_c/Z)^{2/3}} \approx 15 \tag{A.5}$$

which, for reasonable values of (m^*/m), gives an unacceptable high values of electron per Ni atom. Similarly, for $Al_3Ni_{20}B_x$, these calculations give an unacceptable value of 100–700 electrons per unit formula. Nevertheless, and particularly due to the absence of band structure calculation on $Al_3Ni_{20}B_x$, these free-electron expressions serve as a good starting criterion for the rationalization of the electronic properties.

On the other hand, the magnetic susceptibility of nonmagnetic intermetallics is usually taken to be a sum of various contributions such as orbital, Landau (diamagnetism), and Pauli (paramagnetism) terms. In particular if a measured curve exhibits a positive susceptibility (and that the Pauli term is the only one) then for the non-enhanced limit and $T < T_F$, this contribution is related to $N(E_F)$ as:

$$\chi_o = 2\mu_B^2 N(E_F), \tag{A.6}$$

where μ_B is the Bohr magneton.

Finally, the measured resistivity $\rho(T)$ is taken to be a sum of a residual term ρ_0 and a temperature-dependent contribution which can be approximated by the Bloch–Grüneisen expression [16]:

$$\rho(T) - \rho_0 = (4\pi)^2(\lambda\omega_p^{-2})\omega_D\left(\frac{2T}{\theta_D}\right)^5 \int_0^{\theta_D/2T} \frac{x^5}{\sinh(x)^2}\,\mathrm{d}x \tag{A.7}$$

where λ is the electron–phonon coupling, ω_p is the Drude plasma frequency ($\omega_p^2 = (4\pi e^2 n)/m$; factors have their usual meaning), and ω_D is the Debye phonon frequency. As is the usual practice [e.g. 17], the resistivity is taken to be governed by the variation in ρ_0, (λ/ω_p^2), and θ_D. If θ_D is taken from specific heat analysis and ρ_0 is determined from the extrapolation to lower temperatures, then the only free parameter is the ratio (λ/ω_p^2) which reflects the influence of both the electronic structure and the strength of the scattering process: both parameters are expected to vary smoothly across the homogeneity range of $Al_3Ni_{20}B_x$.

References

[1] E. Schmid, G. Petzow, G. Effenberg, in: Ternary Alloys, vol. 3, VCH Verlagsgesellschaft, Germany, 1989, p. 201.
[2] P. Rogl, Ternary Alloy Systems, Crystallographic and Thermodynamic Data, Phase Diagrams (Materials Science Intern. Services GmbHEditor: Effenberg, G., Ilyenko, 2004), vol. IV/IIA1 of Landolt-Börnstein, New Series, chap. Aluminum–Boron–Nickel, p. 67.
[3] C. Campbell, U. Kattner, J. Phase Equilib. 20 (1999) 485.
[4] H. Hillebrecht, M. Ade, Angew. Chem. Int. Ed. 37 (1998) 935.
[5] V. Raghavan, J. Phase Equilib. Diffus. 27 (2006) 486.
[6] I. Hase, Phys. Rev. B 70 (2004) 033105.
[7] D. Hackenbracht, J. Kubler, J. Phys. F 10 (1980) 427.
[8] N.I. Kulikov, A.V. Postnikov, G. Borstel, J. Braun, Phys. Rev. B 59 (1999) 6824.
[9] H.H. Stadelmaier, R.A. Draughn, G. Hofer, Z. Metallk. 54 (640) (1963) (in German).
[10] B. Albert, H. Hillebrecht, Angew. Chem. Int. Ed. 48 (2009) 8640.
[11] H. Hirota, J. Phys. Soc. Japan 23 (1967) 512.
[12] M.A. Taylor, Proc. R. Soc. Lond. 78 (1961) 1244.
[13] E.S.R. Gopal, Sepecific Heat at Low Temperatures, Plenum Press, New York, 1966.
[14] T. Chraska, J. Lasek, P. Chraska, Mater. Sci. Eng. A 244 (1998) 263.
[15] G.A. Botton, G.Y. Guo, W.M. Temmerman, C.J. Humphreys, Phys. Rev. B 54 (1996) 1682.
[16] P.B. Allen, J.R. Chelikowsky, S.G. Louie, in: Quantum Theory of Real Materials, Kluwer, Boston, 1996, p. 319.
[17] D. Mandrus, B.C. Sales, R. Jin, Phys. Rev. B 64 (2001) 012302.